This is a repository copy of *Simulations and Measurements in Scanning Electron Microscopes at Low Electron Energy.*.

White Rose Research Online URL for this paper:
https://eprints.whiterose.ac.uk/106087/

Version: Accepted Version

Article:

Simulations and Measurements in Scanning Electron Microscopes at Low Electron Energy

Christopher G.H. Walker,[1] Luděk Frank,[2] and Ilona Müllerová[2]

[1]Department of Electronics, University of York, Heslington, York, United Kingdom
[2]Institute of Scientific Instruments, Brno, Czech Republic

Summary: The advent of new imaging technologies in Scanning Electron Microscopy (SEM) using low energy (0–2 keV) electrons has brought about new ways to study materials at the nanoscale. It also brings new challenges in terms of understanding electron transport at these energies. In addition, reduction in energy has brought new contrast mechanisms producing images that are sometimes difficult to interpret. This is increasing the push for simulation tools, in particular for low impact energies of electrons. The use of Monte Carlo calculations to simulate the transport of electrons in materials has been undertaken by many authors for several decades. However, inaccuracies associated with the Monte Carlo technique start to grow as the energy is reduced. This is not simply associated with inaccuracies in the knowledge of the scattering cross-sections, but is fundamental to the Monte Carlo technique itself. This is because effects due to the wave nature of the electron and the energy band structure of the target above the vacuum energy level become important and these are properties which are difficult to handle using the Monte Carlo method. In this review we briefly describe the new techniques of scanning low energy electron microscopy and then outline the problems and challenges of trying to understand and quantify the signals that are obtained. The effects of charging and spin polarised measurement are also briefly explored. SCANNING 9999:1–17, 2016. © 2016 Wiley Periodicals, Inc.

Key words: Monte Carlo modeling, scanned probe, computer simulation, electron-solid interactions, surface analysis

Introduction

Traditional Scanning Electron Microscopes (SEMs) in which finely focused beams are swept across sample surfaces have typical energies of 10–30 keV. However, there is a growing interest in the use of low energy electrons in the study of materials. Different areas of science have different meanings for low and high energy. For instance, electron microscopists tend to regard 2 keV as "low energy" while surface scientists think of 2 keV as "high energy." In this report, we will tend to consider the microscopists view point and take "low energy" to be less than 2 keV.

New techniques such as the cathode lens (Frank *et al.*, 2007) have introduced the possibility to study materials right down to 1 eV or below in SEMs. Such low energies bring several advantages, such as low radiation damage, improved spatial resolution, reduction in the effects of charging, greater sensitivity to the local electron spin orientation and new contrast mechanisms. However, at these energies, new challenges are presented as the understanding of electron transport in materials is much poorer than at higher energies.

In addition to simulating the low primary beam energies, it is also important to simulate the secondary electrons (SEs) (i.e., those electrons that were previously bound in the material, but have been excited to energies such that they can escape into the vacuum) which are generated from the primary beam electrons. Such electrons typically have energies of just a few eV, but can extend to energies up to several keV. It is important to understand the generation and transport of SEs for a number of technological reasons (Mikaelian, 2001; Dunaevsky *et al.*, 2003; Pivi and Furman, 2003). Although certain Monte Carlo (MC) programs provide the capability to simulate SEs, the lack of inclusion

within the models of the wave nature of the electron and band structure etc. leads one to question the accuracy of such models.

The two main experimental techniques we will consider are the Near Field Emission Scanning Electron Microscope (NFESEM) (Young *et al*., '72; Kirk, 2010) and Scanning Low Energy Electron Microscopy (SLEEM) (Müllerová, '99). Another powerful technique that uses low energy electrons is Low Energy Electron Microscopy (LEEM) (Bauer, '94). LEEM uses an electron gun (15–20 keV), condenser optics and a magnetic deflector before being decelerated prior to striking the sample surface. The sample is held at a high potential such that the electron landing energies are in the range 1–100 eV. LEEM has a spatial resolution in the nanometre range and can be made spin sensitive. However, this technique is not scanning and so falls outside the limits of this review (and this journal). Nevertheless, many of the points made in this review could also be applied to LEEM.

The Near Field Emission Scanning Electron Microscope (NFESEM)

The NFESEM (also known as a Topografiner) has introduced a new way of generating SEs and thus offers the prospect of a new approach to sample characterization at the nanometre scale (Young *et al*., '72; Zanin and Cabrera, 2012). In a NFESEM, a field emission electron source, (which is normally far from the surface in a standard SEM) is brought to within a few nm of a surface (see Fig. 1). A negative voltage is applied to the field emission tip relative to the sample such that electrons are field emitted from the tip and strike the sample. It has been found that the lateral resolution of NFESEM is much better than would have expected from traditional theory of field emission. However, a new theory can

explain the improved resolution (Zanin and Cabrera, 2012). Typical primary beam energies for the instrument are tens of eV, which is sufficient to generate SEs. The tip can then be scanned across the sample to generate an image from the sample current. The reader who is acquainted with the Scanning Tunneling Microscope (STM) (Binnig and Rohrer, 2000) will note the similarities between the NFESEM and STM. The NFESEM has a poorer resolution than that of STM, but NFESEM has the potential to do some characterization of the sample unavailable to STM such as SE generation. Indeed, SE generation and collection has already been demonstrated (Zanin and Cabrera, 2012), and used to acquire electron spin polarization information (Pescia, 2015). Whether it can be used to determine elemental composition has yet to be shown. Due to the high surface sensitivity of the low energy electrons used in NFESEM, the experiment needs to be operated in Ultra High Vacuum (UHV).

Scanning Low Energy Electron Microscopy (SLEEM)

SLEEM achieves a low landing energy for the impacting electrons by using a high voltage (5–10 kV) electron column and then applying a bias to the sample such that the electrons are decelerated between a detector mounted below the electron column and the sample (see Fig. 2). The landing energy is simply the difference between the energy of the electrons leaving the electron column and the specimen bias, i.e.

$$E = e(V_A - V_B) \qquad (1)$$

where E is the landing energy, V_A is the acceleration voltage, V_B is the specimen bias and e is the charge on the electron. The strong decelerating field between the sample and objective lens acts as an extra immersion converging lens (and is called a Cathode Lens (CL))
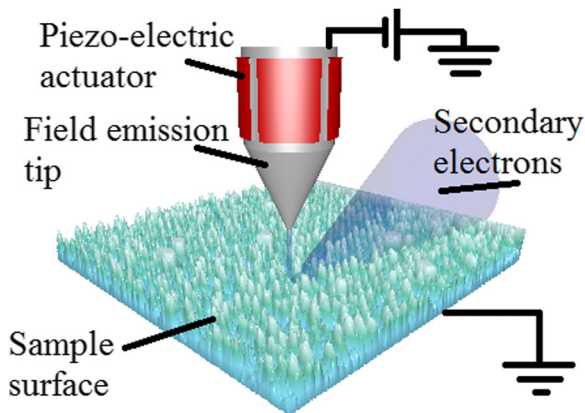

Fig 1.   Schematic of the NFESEM. The tip (gray) is operated in Field emission mode creating an electron current and secondary electrons (blue) which are accelerated away from the tip region by an electric field.
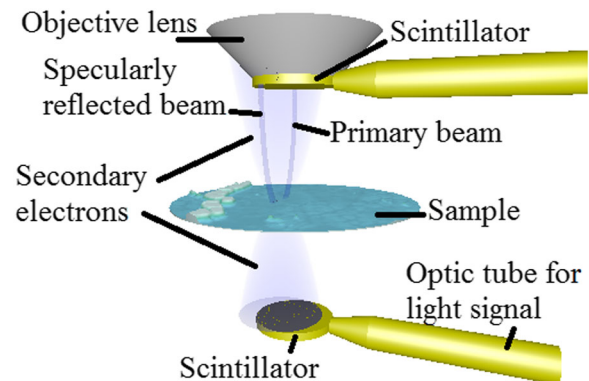

Fig 2.   Schematic representation of the SLEEM. The sample is placed at a high negative potential and the scintillators are earthed.

enabling the spot size to be comparable to that obtained at high energy (Müllerová and Frank, 2003). An important parameter which describes the strength of the CL is the immersion ratio, k, and is the ratio between primary beam energy and the landing energy and is thus given by:

$$k = eV_A/E = V_A/(V_A - V_B) \qquad (2)$$

Backscattered electrons (BSEs) (i.e., primary beam electrons that have been backscattered from the sample) and SEs from the surface are re-accelerated towards the detector which then generates a strong signal in that detector. Since the primary beam is slowed only in the vertical direction, the electrons arriving and leaving the surface travel in parabolic trajectories as indicated in Figure 2. The reflected specular beam will arrive at the top detector as a small spot whereas the excited SEs will have a broad range of electron energies and momenta and so will have a broad spot on the detector.

Some prerequisites are that the sample needs to be flat (units of μm for 1 eV landing energy (Müllerová and Frank, 2007) and the sample can only be tilted by a few degrees. In addition, the beam passes through a small aperture in the scintillator detector which limits the fields of view of the SEM. Despite these minor drawbacks, there are many advantages to SLEEM such as the many new image contrast mechanisms that appear at lower energies (Müllerová and Frank, 2003). The low impact energy results in a much greater surface sensitivity and a dependence on quantum effects. In turn this means that (as is the case for NFESEM) it is best to use SLEEM in UHV conditions. In another novel development, the transmission of low energy electrons through very thin films can be studied by this technique (Müllerová *et al.*, 2011). Figure 2 shows this arrangement for transmission SLEEM. Earlier SLEEM instruments would not have had the lower scintillator.

The Monte Carlo Method

The traditional method to simulate electron transport in SEM experiments is Monte Carlo (MC) (Joy, '91; Dapor, 2003). The MC method was begun by Stanislaw Ulam and John von Neumann studying neutron transport as part of the Manhattan project (Eckhardt, '87). The technique involved the use of random numbers to model complex phenomena which were not easily solved via conventional transport theory (Ziman, '56) involving Partial Differential Equation analysis. If the probability function, p(x) (see Annex) is known, then an answer to the transport problem may be obtained by obtaining an average value by repeated simulations of a large number of particles. "Monte Carlo" was named by Nicholas Metropolis (after the random nature of the games played in the Casinos of that city) as the method was top secret and needed a somewhat obscure title (Metropolis, '87).

Many of the early MC simulations of electron transport used the continuous slowing down approximation (CSDA) (Joy, '95; El Gomati *et al.*, 2008). However, this makes it difficult to know how to assign energies and momenta to SEs generated by the primary electron. In addition, one cannot simulate "straggling" whereby some electrons undergo relatively few inelastic losses and travel much further than the average distance. When one considers electrons suffering discrete losses (Ding and Shimizu, '96; Salvat *et al.*, 2001; Bernal *et al.*, 2015), it is usual to consider that the energy lost by the primary particle is transferred to a SE. In addition, the generation of surface plasmons will lead to many of the SEs being generated at or close to the surface (Khalid *et al.*, 2013). Plasmons are collective oscillations of conduction/valence electrons in an energy range from a few eV to ~30 eV. The bulk plasmon energy (ω_p) is to first order related to the nearly free electron density in the material with the additional possibility of surface plasmons at $\omega_p/\sqrt{2}$. Plasmon loss is in many systems the main mechanism of energy loss but more complex excitations occur in transition and noble metal systems. The MC method does not normally take into account the crystallinity of the sample and its structure is assumed to be amorphous.

In the annex of this paper there is a summary of how random decisions are made in MC simulations by the use of a probability distribution.

In the case of MC simulation of electron transport in materials, we need to simulate two types of random events—Elastic Scattering and Inelastic Scattering.

Elastic Scattering

An electron striking a nucleus has initial velocity v_i and final velocity v_f and scatters through angles θ and φ according to Figure 3. The angle φ has an equal probability between 0 and 2π. Hence if one chooses a random number, r, between 0 and 1. The value of φ will be given by 2πr.

The value of θ is more difficult to determine. The early work using the Born approximation (i.e., the wave function of the incoming electron is approximately the same as the wave function after the scattering event)
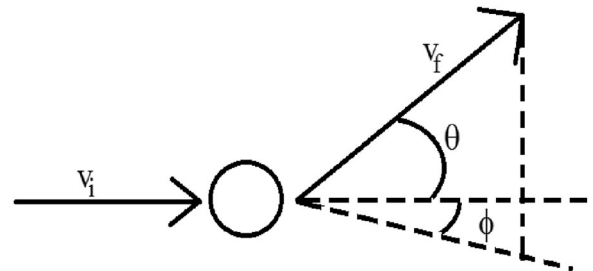

Fig 3.   Elastic scattering of an electron from an atom.

predicts Rutherford like forward dominated scattering, but this has now been superseded by Mott scattering (Mott and Massey, '49) capable of coping with strong and very weak scattering. Figure 4 shows the Mott differential cross-section for elastic scattering for four different energies for the element Cu (Jablonski *et al.*, 2010). Note the vertical scale is logarithmic so there is a much greater probability of scattering with only a small angle of deflection than one of (for example) 90° or more. Determination of the curves is quite time consuming computationally. Hence the curves are calculated prior to the main MC calculation. When an electron has an intermediate energy between two tabulated energies, the result is interpolated between the elastic scattering curves above and below the energy of the electron. Generally this procedure is good enough as any inaccuracies are averaged away due to the multiple scattering that the electron undergoes. However, it should be noted that under certain circumstances such an interpolation procedure may lead to unacceptable inaccuracies. If the tabulated energies were at 100 and 200 eV, then the curve for 150 eV should be intermediate between these two values. However, upon inspection of Figure 4 the reader will notice that the actual 150 eV curve has a much sharper dip near to a scattering angle of 72° than either the 100 or 200 eV curve. If one were studying the elastic peak reflected from a surface (i.e., little or no multiple scattering) near these energies and angles, the MC simulation could provide the wrong results. This would apply especially for very thin films (e.g., free standing 2D materials). In principle, the dips that one sees in the Mott scattering could be used to characterise a sample. However, in a sample consisting of several elements, the dips in scattering intensity at certain angles will be dominated by scattering from other elements with no such dip in scattering intensity at the same angles. Hence
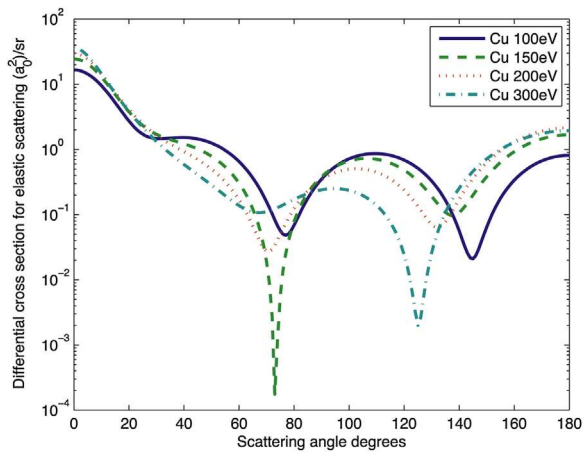
the measured curve of scattering versus angle will appear much smoother in such samples. Nevertheless, one has to be careful when interpolating pre-calculated curves in MC since the statistical nature of the technique can hide problems and their causes. A previous example of this was reported by El Gomati *et al.* (2008).

Inelastic Scattering

Continuous slowing down approximation

In order to improve the speed of calculation, a simple approximation for the inelastic losses can be undertaken. This is to assume that the electrons travel in straight lines between elastic collisions and that the electrons lose energy in a continuous manner between those elastic collisions. This approximation is known as the Continuous Slowing Down Approximation (CSDA). A well-known formula for determining the rate of stopping power, S, of the electrons is due to Joy and Luo ('89) where they define the stopping power as

$$ S = -785 \frac{Z}{AE} \ln(\frac{1.166E}{12.35Z} + 1.174) eV/\mathring{A} \qquad (3) $$

where Z is the atomic number, A is the Atomic mass, ρ is the density (g/cm^3) and E is the electron energy (eV). Although the CSDA is a useful approach to speeding up MC simulations, there are certain effects which cannot be simulated when one takes this approach. These would include the elastic peak of reflected primary electrons. If studying the electrons passing through a thin film, then all electrons will have lost a minimum amount of energy whereas in reality there would be some electrons that could travel quite far without having lost much energy—this is also known as "straggling." Hence a better approach is to simulate discrete inelastic losses. At low electron energies there are significant uncertainties in the stopping power and the elastic scattering. Walker *et al.* (2014) have studied how the errors in the stopping power and elastic scattering cross-sections propagate to the errors in backscattering coefficients and find good agreement with the electron transport theory of Tilinin and Werner ('93).

It should also be noted that it is difficult to simulate secondary electron emission (SEE) using CSDA as one normally uses the energy lost in the discrete energy losses to provide the energy for the generation of the SEs.

Discrete inelastic losses

In order to provide more accurate simulation of the electron transport, it is necessary to simulate each inelastic loss individually. This is usually carried out by making use of the optical dielectric function, $\varepsilon(\omega)$, (where $\hbar\omega$ (=T) is the energy loss). The use of the dielectric function to describe inelastic scattering was suggested by Fermi ('40) and the field was further

Fig 4. Elastic Scattering cross-sections (units of Bohr radius squared per steradian) for Cu between 100 and 300 eV (Jablonski, Salvat and Powell, NIST Electron Elastic-Scattering Cross-Section Database-Version 3.2 2010).

advanced by Ritchie ('59). Powell ('67) suggested using optical data obtained from experiments in modeling inelastic scattering. As a result, the models of Ritchie were developed to determine the Optical Energy Loss Function (OELF) for energy loss T and momentum transfer q (Ritchie and Howie, '77; Penn, '87; Ashley, '88). Ritchie and Howie ('77) proposed a quadratic dispersion relation for the Drude energy coefficient. The OELF can be described by a sum of Drude-type Energy Loss Functions (e.g., Akkerman *et al.*, 2005). Penn ('87) and Ashley ('88) introduced an approach whereby the summation over a limited number of terms is replaced by an integral (i.e., infinite number of terms). The optical dielectric function only considers values for zero momentum transfer (i.e., $q = 0$). Estimates of the optical dielectric function for non-zero values of q can be determined by extrapolating the optical dielectric function into the rest of "q-space" using Drude/Drude-Lindhard models (Yubero *et al.*, '96; Werner *et al.*, 2009). Many models do not show a broadening of the loss function as q increases which is expected from experiment (Batson and Silcox, '83). This disagreement can be reduced by adding a term which makes the broadening dependent on q (Emfietzoglou *et al.*, 2005). The Mermin approach (Mermin, '70) to a model dielectric function uses a free electron model where the width of the loss peak is dependent on q. This model has recently been explored by Vos (2016) for a range of momentum transfer values. It should be noted that the dielectric function description of inelastic electron scattering assumes that the Born approximation holds. At lower electron energies, the Born approximation is expected to be less valid. Exchange and correlation (XC) effects have been studied recently (Emfietzoglou *et al.*, 2012, 2013) and the authors find that the XC corrections cause a larger reduction in the inelastic cross-section compared to other commonly used approximations. This implies that including XC effects should increase theoretical values for the inelastic mean free path (IMFP).

A plot of the imaginary part of the inverse of the dielectric function for zero momentum transfer (i.e., the OELF) can be determined from optical measurements (Palik, '98) and is shown in Figure 5 for the case of Si. Palik ('98) provides the data up to 2 keV for Si and this has been extended to 10 keV by assuming the curve has the same slope in Figure 5 before and after the K shell edge at ∼1.8 keV. Valentin *et al.* (2012) used photo-absorption data to determine the dielectric function in this range.

Direct measurements of the dielectric function for $q \neq 0$ can be carried out using Inelastic X-ray Scattering (IXS) and Electron Energy Loss Spectroscopy (Egerton, '96; Hayashi and Udagawa, 2011). Measurements have been carried out using IXS for H_2O (Hayashi and Udagawa, 2011) and Si (Weissker *et al.*, 2010) and show that there are significant deviations from the simple
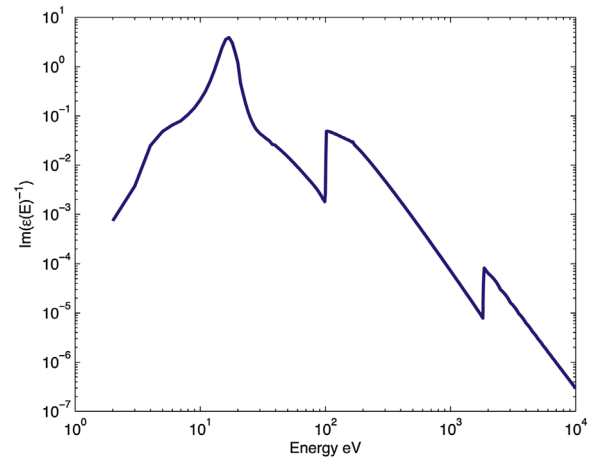

Fig 5. Imaginary part of the inverse of the Optical Dielectric Function of Si from Palik ('98).

quadratic rule. Another approach to obtaining the dielectric function at $q \neq 0$ is to use Time Dependent Density Functional Theory (TDDFT). Weissker *et al.* (2010) find good agreement between TDDFT calculations (using Time Dependent Local Density Approximation—TDLDA) and IXS measurements. However, TDLDA does not include lifetime effects of electrons and holes and these needed to be taken into account separately.

The Differential Inverse Inelastic Mean Free Path (DIIMFP) is the energy loss probability in an individual collision (see Werner, 2001). It has been determined here from Optical Dielectric data (Palik, '98) using the approach described by Werner (2001) for 500 eV electrons and is shown in Figure 6. In order to determine an energy loss from an inelastic event, the function in Figure 6 is normalised such that the total area under the curve is 1 and then integrated. The energy loss can then be determined using a random number between 0 and 1 and selecting the corresponding energy which has a
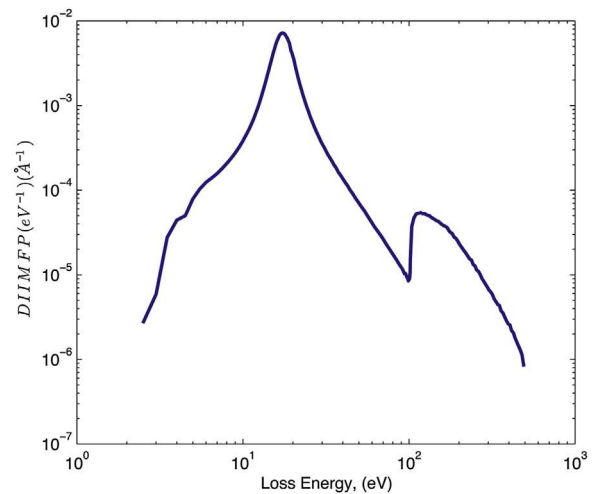

Fig 6. Differential Inverse Inelastic Mean Free Path for 500 eV electrons in Silicon.

cumulative distribution value equal to the chosen random number (i.e., in the same manner that the scattering angle is chosen). Since the determination of curves such as that shown in Figure 6 are time consuming to determine, they are calculated before running the MC simulation and as in the case of elastic scattering, the results are tabulated. For electrons of intermediate energies, a weighted average DIIMFP curve is determined from the DIIMFP curves for electron energies above and below the electron energy. Since the DIIMFP curves vary only slightly with energy, tabulation errors are not expected to be significant. The energy lost in the inelastic process is normally transferred to a SE in the MC simulation. Hence Figure 6 shows the distribution of starting energies of SEs for primary electrons of 500 eV. The slight oscillations below the L edge at about 100 eV are due to an artefact of the mathematical process but do not greatly affect the SE background or slowing down of the primary electrons. The new direction of the primary electron can be determined from a further random number and the direction of the SE can be determined from conservation of momentum or chosen randomly (Dapor, 2003).

The electron mean free paths

The inelastic mean free path (IMFP) is the average distance travelled between inelastic (i.e., some energy loss) events. The elastic mean free path (EMFP) is the average distance travelled between elastic (i.e., no energy loss) events. The mean free path (MFP) is generally regarded as the distance between an event whether it is inelastic or elastic (Barrett *et al.*, 2005). The transport mean free path (TMFP) can be regarded as the distance over which the direction of the scattered electrons is randomized. The TMFP depends on both the IMFP and EMFP, but no general formula exists for the TMFP for low energy electrons in materials. There are a number of other measures of electron transport through materials (e.g., Attenuation Length) and these are defined and discussed by Jablonski and Powell ('99). The IMFP is generally regarded to reach a minimum between 50 and 100 eV and then to start increasing as the electron energy reduces. This has often been depicted in the form of a "Universal Curve" as determined by Seah and Dench ('79) (see Fig. 7). More recent work by Tanuma *et al.* (2005) on calculated forms of the IMFP abandon the concept of a "Universal Curve," but the form of the curve is broadly similar for all elements. However, recent measurements of the IMFP using XANES on Cu suggest that the IMFP in the region of 20–120 eV is smaller than predicted (Bourke and Chantler, 2010) by either the "Universal Curve" (Seah and Dench, '79) the TPP-2 M formula (Tanuma *et al.*, 2005) or other methods to determine the IMFP. Zdyb and Bauer (2013) studied thin films of Fe on W using Spin Polarised LEEM. They also find a lower IMFP than is theoretically expected and find
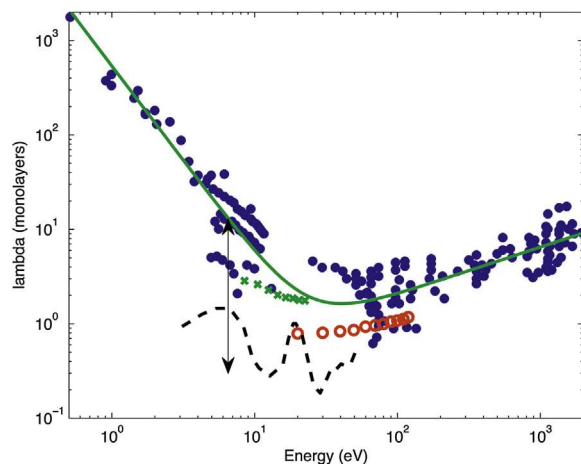

Fig 7.   The "Universal Curve" for the Inelastic Mean Free Path from Seah and Dench ('79). Energy is measured above the Fermi level. Blue dots are data as used by Seah and Dench ('79), Green line is fitted "Universal Curve," green crosses are from Zdyb and Bauer (2013) and red circles are from Bourke and Chantler (2010). The double headed arrow shows the range of IMFP values determined from SE emission experiments (Walker *et al.*, 2008). The dotted black line is from Barrett *et al.* (2005). The IMFP results from Zdyb and Bauer (2013), Bourke and Chantler (2010), Walker *et al.* (2008) and Barrett *et al.* (2005) have been converted from distance to monolayers and where necessary converted from energy above the vacuum level to energy above the Fermi level.

a much slower dependence with energy for the IMFP in the region 8–16 eV than is predicted. In addition, Walker *et al.* (2008) studied SEE from 24 different elements and were able to make an estimate of the IMFP of the SEs. The results of Bourke and Chantler (2010), Zdyb and Bauer (2013), and Walker *et al.* (2008) have been added to Figure 7. It is assumed that the SEs had an energy of 2 eV for the results of Walker *et al.* (2008). Lin and Joy (2005) also carried out a similar analysis of IMFPs to Walker *et al.* (2008) and found a similar range of results. Walker *et al.* (2008), El-Gomati and Walker (2014), El-Gomati *et al.* (2011) also suggest that a proportion of the SEs could be generated by decaying surface plasmons and so are generated at or very close to the surface. This agrees with the coincidence results of Khalid *et al.* (2013) resulting in smaller measured IMFPs. Nevertheless, a significant proportion of the SEE has to come from the bulk, otherwise the trends seen across each of the Transition Metal series would not be apparent (see the later section "Scattering due to empty d-states"). Hence, there is increasing evidence that in the low energy range, the electron IMFP is smaller and has a flatter energy dependence than is suggested by a "universal curve" or values determined from dielectric theory (Bourke and Chantler (2010)) and it would seem some further research of the IMFP in this region is required.

The Elastic Mean Free Path (EMFP) does not reach a minimum, but reduces more than the IMFP as the electron energy is lowered (Jablonski *et al.*, 2010). The

elastic scattering is due to diffraction of the crystal potential for certain values of energy and wave vector which are band gaps in the unoccupied states and diffraction minima in the EMFP can occur, which are very much material dependent (Barrett *et al*., 2005). In a study of transmission of low energy electrons, Frank *et al*. (2015) find that the transport mean free path (TMFP) continues to decrease even for the lowest electron energies considered of 1 eV. In a study of a graphite overlayer on Si, diffraction structure in the MFP appeared as intensity minima of the Si2p photoemission signal was found to reflect band gaps in the unoccupied states of graphite (Barrett *et al*., 2005). However, the transmission data of Frank *et al*. (2015) reveal no such structure in graphene, although this could be due to a relatively coarse step in energy, so that fine oscillations below 8 eV could not be revealed. Since the high levels of elastic scattering at low primary beam energy can be attributed to diffraction effects, it is necessary to consider how crystallography can be introduced into electron transport simulations in materials.

Simulation of Secondary Electrons

There have been a number of programs developed to simulate SEE (Ding and Shimizu, '96; Dapor, 2003; Villarrubia *et al*., 2007; Kieft and Bosch, 2008; Valentin *et al*., 2012). SEM images have also been simulated (Li and Ding, 2005; Kieft and Bosch, 2008; Li *et al*., 2011), although this is computationally intensive and parallel computation is preferred (Li *et al*., 2011). However, most MC simulations consider only the higher energy primary and BSEs with serial computation (Starý *et al*., 2008; Walker *et al*., 2008). CASINO has recently introduced SE simulation (Demers *et al*., 2011). There have also been two approaches taken to introduce SE simulation using the package GEANT4 (Kieft and Bosch, 2008; Bernal *et al*., 2015). The first of the simulations that use GEANT4 is used to simulate low energy electrons in water as part of the Geant4-DNA project (Bernal *et al*., 2015). The MC code by Valentin *et al*. (2012) is based on the GEANT4-DNA project (Bernal *et al*., 2015) is only available for Si and does not simulate electrons lower than the plasmon energy of Si. However, the code can be freely downloaded if one installs the GEANT4 development code and the code by Valentin *et al*. (2012) can be found under the "microelectronics" subdirectory. Valentin *et al*. (2012) relied on the work of Akkerman *et al*. (2005) by modeling an extended-Drude expression to the Optical Energy Loss Function (see Fig. 5). Akkerman *et al*. (2005) used fifteen peaks for their model whereas Valentin *et al*. (2012) found that six were sufficient. The second code that uses the Geant4 package is by Kieft and Bosch (2008), This code simulates electrons in many

materials and down to energies to just below the work function of the material, but is not yet available publicly. These authors interpolate between elastic scattering cross-sections at high energy and electron transport properties of thermal electrons to determine the behavior of electrons with intermediate energies. Schreiber and Fitting (2002) describe an approach involving electron interaction with phonons, inter-valley and inter-band scattering and impact ionization for the case of SiO_2. Other effects that need to be taken into account, especially as the electron energy reduces, are Acoustic Phonon, Polar Optical Phonon, Non-Polar Optical Phonon, Equivalent Inter-valley Phonon, Non-equivalent Inter-valley Phonon, Ionized Impurity, Carrier–Carrier: (electron–electron, hole–hole and electron-hole interactions) and plasmon generation and decay. These effects are taken into account by MC programs that simulate electron transport in semiconductor devices (Hess, '91) but many are not taken into account for MC simulations of the much higher energy electrons in simulations of experiments carried out in SEMs. Trying to include these effects would bring a great deal of extra complexity to the MC simulations. Current experiments are unlikely to be sensitive to these extra effects, but with careful study of the SE background at low electron energy, this may change.

Secondary ElectronsMeasurement/Simulation Comparison

It was noted by Sickafus ('77) that the intensity of the SE background could be accurately described by a curve of the form AE^{-m} where A and m are positive constants and E is electron energy. This empirical result has been shown to be valid for many different materials (Greenwood *et al*., '94). It is expected from theory that the value of m should be around one with deviations from this value caused by elastic scattering which increases m as it becomes stronger and the energy dependence of the IMFP which decreases m as it becomes steeper (Matthew *et al*., '88).

One test of SE simulation using MC would be to see if the simulated SE background also follows a similar law and whether the same value of m is found for each material. The results of such a comparison is shown in Table I where three programs were used to generate the SE spectra (Kieft and Bosch, 2008; Walker *et al*., 2008; Valentin *et al*., 2012). Clearly the simulated results from the program of Kieft and Bosch (2008) underestimate the value of m as compared to the experimental measurements of Greenwood *et al*. ('94). The program of Walker *et al*. (2008) was adapted to include discrete energy losses and SE generation for electron energies in the range 5 eV–20 keV. The results of the modified program of Walker *et al*. (2008) tend to overestimate m as compared to the measured values. However, comparison with the

TABLE I   Measured and simulated values of m from the Sickafus empirical law for describing the secondary electron background

Element	Measured (m)	Simulated (m)	Simulated (m)	Simulated (m)
Al	0.67	0.42		
Si	0.67	0.39	1.5	0.96
Ti	0.81	0.20		
Cr	0.87	0.38		
Fe	0.94	0.39		
Cu	1.10	0.29	1.6	
Ge	1.15	0.18		
Ag	0.80	0.41	1.3	
Sn	0.81	0.43		
Ta	0.88		1.2	
W	0.90	0.52		
Pt	0.95	0.56	1.0	
Au	0.97	0.55	0.9	

Column 1 = results of Greenwood et al. ('94), column 2 = results of Kieft and Bosch (2008), column 3 = simulated results using MC model of Walker et al. (2008), and column 4 = simulated result of Valentin et al. (2012).
Errors are ~0.01 for measured results and ~0.03 for simulated results.

slope of the optical energy loss function for each element (see Fig. 5 for the case of Si) and knowing that the slope should reduce by about one for the SE background, the results are about what should be expected. Note that the slope of the line in Figure 5 (in a log–log plot) in the region 300–1,800 eV has a value of about 2.7. This is higher than the slope of the measured SE background, but the slowing down of the SEs as they pass through the material will cause a lower value of the slope for the SE background (Matthew et al., '88). Dapor (2003) reports a value of m for SE background of Cu excited by positrons of about two in close agreement with the experimental results of Overton and Coleman ('97). Dapor (2003) also points out that such positron based experiments are uncontaminated by the spectrum from the BSEs which would have a tendency to reduce the measured value of m. Goto et al. ('94) carried out experiments to determine the Auger electron spectra very accurately at a variety of different beam energies and materials. Ding et al. (2004) compared MC simulations with the dataset from Goto et al. ('94) and found good agreement, although differences can be seen at low primary beam energy near to the elastic peak. It would be a useful exercise for other MC simulations to carry out a similar comparison. However, as shown by Walker et al. (2016), data acquired from forward scattering direction can be in error if the elastic and inelastic scattering cross-sections are not up to date. Hence a similar experiment to Goto et al. ('94) but studying the electron spectrum after traveling through a thin film would represent a new challenge to MC simulations.

SEs are traditionally regarded as those electrons whose energy is less than 50 eV and BSEs are those electrons which have energies above 50 eV. MC simulations of BSEs show a consistent underestimate of the measured signals especially for high Z materials and low primary beam energy (Walker et al., 2008). This underestimate is probably due to not taking into account the contribution of SEs to the BSE signal. When the SEs are included in the simulation, a much better agreement is found (El-Gomati and Walker, 2014). Measurement of the Secondary Electron Yield (SEY or δ) can provide information regarding the IMFP of the SEs (Walker et al., 2009). This has led to some new insight into the scattering processes that SEs undergo (see section on scattering due to empty d-states). Since the SE background is largely featureless, there are difficulties in determining the transport properties of SEs within solids. A route to discovering more about the generation and loss processes is to conduct coincidence experiments (Khalid et al., 2013; Werner et al., 2013).

Walker et al. (2008) showed significant changes in the SE yield between as-inserted and cleaned samples. Since, most surfaces in SEMs are not cleaned, one can assume that the total SE yield will be dominated by surface contamination and considerably hinder quantification efforts.

Cazaux (2010) has highlighted that there is a wide disparity between the values of the maximum in the SEY (or δ_{max}) as a function of energy for many different materials as reported by many different authors and that this is most probably explained by variations in the SEE with the work function. The presence of small amounts of contaminants make a large change in the work function and this significantly affects the escape probability of the SEs.

Scattering Due to Empty d-states

Experiments involving low energy electrons carried out on magnetic materials showed an enhanced spin polarization of the emitted electrons (Siegmann, '92; Schonhense and Siegmann, '93). This spin polarization has been attributed to electrons with different spin directions undergoing different scattering rates (Siegmann, '92). The amount of scattering that an electron undergoes is dependent on the number of empty d-states. In magnetic materials, there are different numbers of empty d-states for spin up and spin down electrons. This results in different scattering rates and a different mean free path (MFP) for each spin type. Recently it was recognised that the scattering due to empty d-states would also affect the emission of SEs from all metallic surfaces (Walker et al., 2008). This was determined by looking at the maximum SE intensity as the primary electron beam energy was varied (see Fig. 8) and studying the energy at which this maximum occurred (see Fig. 9). Since the number of empty d-states reduces for each element as each transition metal (TM) series is crossed, so the electron scattering will reduce and the MFP increase. Hence, this should give rise to a rising SEE
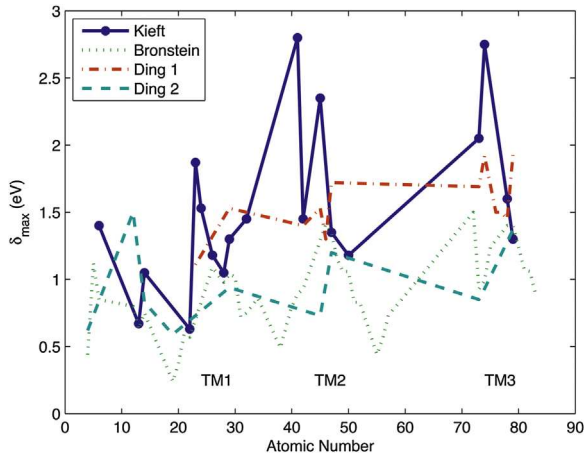
Fig 8. The maximum value of SE yield (δ_{max}) (as the primary energy is varied) as a function of atomic number for (Kieft and Bosch, 2008) (labelled Kieft), (Bronstein and Fraiman, 1969) (labelled Bronstein) and (Ding and Shimizu, '96) (labelled Ding1 and Ding2, where Ding1 assumes SEs excited from the top of the valence band and Ding2 assumes SEs excited from the whole of the valence band). TM1, TM2, and TM3 = first, second, and third transition metal series.

as one crosses each TM series and indeed this is what is observed. Since the work function (WF) of the TM elements also increases across each TM series, then one might expect the opposite to be observed. The unexpected correlation of WF and SEY first noted by McKay ('48) was explained by Baroody ('50) by using the argument that there were more electrons in the valence band for metals with a higher WF. The greater number of valence electrons implied that a greater number of these could be excited as SEs. However, it now
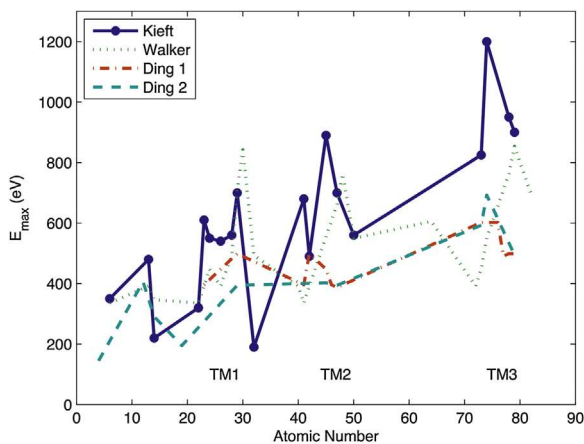

Fig 9. Energy of the primary beam at which the maximum in SE intensity occurs (E_{max}) as a function of atomic number for (Kieft and Bosch, 2008) (labelled Kieft), (Walker, *et al.*, 2008) (labelled Walker) and (Ding and Shimizu, '96) (labelled Ding1 and Ding2, where Ding1 assumes SEs excited from the top of the valence band and Ding2 assumes SEs excited from the whole of the valence band). TM1, TM2, and TM3 = first, second, and third transition metal series.

seems that the IMFP of the SEs plays a role in this correlation. The reduction in SEE due to increases in WF is outweighed by increases in the IMFP in the case of the TMs. It should also be pointed out that the EMFP may also be very short at low energies and may even dominate the TMFP. However, since the effect of empty d-state scattering can be clearly seen for the TMs, then one can say that the IMFP is likely to be as short, or shorter than the EMFP for the TMs. The corresponding values of E_{max} and δ_{max} as calculated by the program of Kieft and Bosch (2008) and from the results of Ding and Shimizu ('96) are also plotted in Figures 8 and 9. There is no discernible correspondence between measured and MC results in each case. The IMFPs estimated by Walker *et al.* (2008) and by Lin and Joy (2005) for the TMs are considerably shorter (between 0.1 and 1 nm) than the "Universal Curve" shown in Figure 7 would suggest. If the depth from which SEs can escape the material is larger, then the SE yield will also be larger. Hence it is important to make sure that the IMFP is correctly modelled in MC simulations for low energy electrons if one is to have good quantitative comparisons.

Simulating SEE is not easy and that the accuracy becomes worse as the energy drops. In addition, the SEY is easily affected by surface contamination. Hence in order to improve our understanding of SEE and to assess whether SEE models are improving one possible approach would be to measure and simulate SEE at higher electron energies. Hence if the total SEY for electrons between two higher energies (e.g., 50 and 100 eV) one would hope that better agreement between experiment and simulation could be observed. The comparison between experiment and theory could then be studied at lower and lower energies as the MC simulation models improve. However, this approach represents an experimental challenge due to the low signal currents that would be obtained.

The effects due to empty d-state scattering should be manifested in the dielectric properties. Ding and Shimizu ('96) simulated the SEE of several elements using the optical dielectric properties (where momentum transfer is zero) and extended the data into non-zero momentum transfer by using nearly free electron (NFE) theory. Their simulated results do not seem to show evidence of scattering due to empty d-states. Indeed there is no trend across each TM series for the optical dielectric function. Hence, it is believed that the empty d-state scattering will be manifested in the dielectric function for non-zero momentum transfer. Use of NFE theory cannot be relied on to provide non-zero momentum transfer values for empty d-state scattering. Calculating the dielectric function for non-zero momentum using Time Dependent Density Functional Theory (TDDFT) would be a way forward. This has been done for the case of Silver (Alkauskas *et al.*, 2010) and Si (Weissker *et al.*, 2010). However as Weissker *et al.* (2010) point out their TDDFT does not take into

account the lifetime of electrons and holes and these need to be handled separately. Zhukov *et al*. (2003) used Full Potential (FP) DFT techniques to determine quasi particle lifetimes in Ag and obtain better agreement than pseudopotential approaches. However using the FP approach is more computationally expensive.

Simulating the Effect of Crystallography

All MC simulations of electron transport in SEMs assume that the material under bombardment is amorphous (e.g., Ding and Shimizu, '96; Dapor, 2003). However, the influence of crystallography on the emerging BSEs and SEs is unmistakeable (Kite *et al*., 2002; Pokorná *et al*., 2012) and this becomes more important for lower energy electrons. The measurement of Electron Back-Scatter Diffraction (EBSD) patterns provides a method to determine the crystallographic orientation of crystal grains under the beam (Wilkinson and Britton, 2012). EBSD patterns have been simulated by Winkelmann *et al*. (2007) by first calculating the trajectories of electrons in an amorphous material using MC. Then the trajectories are modified determining the diffraction of electron waves by the crystal lattice. Hence, the MC calculation does not include any crystallographic effects, but this the MC output is modified later.

Traditionally, an approach to understanding crystallography of surfaces is Low Energy Electron Diffraction (LEED) operated at primary beam energies between 50 and 400 eV. The LEED spectra can be modelled using dynamical LEED theory with multiple scattering (Pendry, '74). Very Low Energy Electron Diffraction (VLEED) operates at lower energies (typically up to 40 eV) and formerly suffered from difficulties in interpretation due to the effect of the electrons interacting with the empty density of states. However, recent advances have allowed much improved interpretation of VLEED spectra and Low Energy Electron Microscopy (LEEM) images (e.g., see Krasovskii and Strocov, 2009; Flege and Krasovskii, 2014). This new approach of simulating low energy electrons makes use of the band structure as determined by density functional theory (DFT) and Bloch waves and is therefore fundamentally different from the MC approach. Feenstra and Widom (2013) have recently applied a similar method to Krasovskii and Strocov (2009) (but more approximate) by using the wave-function data from the Density Functional Theory (DFT) program VASP—see Hafner (2008). They have also made available much of the code they used to determine the electron reflectivity and transmissivity through thin films (Feenstra and Widom, 2015). This has opened the way for many to duplicate this approach using VASP or other DFT programs (e.g., Clark *et al*., 2005; Gulans *et al*., 2014; Elk, 2016). Gao *et al*. (2015) have extended the approach to include inelastic effects. Much of the structure that is observed in the intensity versus energy structure that one obtains from these calculations, one could not hope to see in a traditional MC simulation because of the lack of crystallographic information and the lack of inclusion of quantum or wavelike effects.

Charging Effects

One of the principal problems for insulators in SEM is that of charging of the sample (Reimer, '85). This leads to image distortion, electrical discharges etc. Charging can be tackled by a number of approaches such as coating the sample with a conductive film, lowering the primary beam energy (Cazaux, 2004, 2005; Khursheed, 2010), tilting the sample or modifying the scan rate or increasing the gas pressure so that ions are generated by electron collisions with molecules, which compensate the charge (Ji *et al*., 2005). Other approaches include heating the sample, or using UV radiation to detrap electric charge (Cazaux, 2004).

Using a lower primary beam energy means that reducing charging is an important aspect of using low energy electron beams. The idea behind lowering the primary beam energy is based on the fact that at certain primary beam energies there is a balance of electron charge going into the sample and electron charge being emitted from the sample (i.e., when the SEY (δ) plus backscattering coefficient (η) is equal to 1). However, such balances change with topography (otherwise there would be no SEM image!) and hence this will not completely eliminate charging, only reduce it. In addition, as pointed out by many authors, many charges are trapped beneath the surface and simply balancing electric charge leaving and entering the surface is far too simplistic (Cazaux, 2004; Reimer, '85; Amlaki *et al*., 2011). However, the method of reducing the beam energy does seem to have the effect of reducing charging and a method which measures the mean rate of charging and its dependence on landing energy was introduced by Frank *et al*. (2001). The method enables the energy for minimum damage within a given field of view.

A vector scanning technique (Thong *et al*., 2001) has also been proposed which results in relatively long times before the primary beam revisits the same or nearby locations on the sample. This is carried out by introducing an "interlace factor" which causes a large step between one pixel being analysed and the next. The vector scanning approach requires rapid settling times for the scanning system. In addition, the vector scanning system would not be appropriate for Scanned Probe techniques such as Scanning Tunnelling Microscopy (STM) or the NFESEM. This is because the tip would have to be moved to a new location to perform a new measurement at high speed with the beam current switched off. This would lead to a high probability of a tip crash.

Simulation of charging has been undertaken by various authors (Ganachaud and Mokrani, '95; Thong *et al.*, 2001; Grella *et al.*, 2004; Cornet *et al.*, 2008; Fitting and Touzin, 2010; Li and Zhang, 2010a,b), but in all cases considerable simplifications of the problem have to be undertaken due to the complexity of the problem. Grella *et al.* (2004) used a MC model to determine the charge build-up on the surface and then used the resulting electric fields to determine the trajectories of the electrons in free space. Hence this necessitated the use of a MC simulation and then Finite Element modeling for the electron trajectory modeling in free space. However, Grella *et al.* (2004) do not consider the very complex problem of charge movement through traps. Cazaux (2005) discusses in an analytic approach how the charging builds with time. Such an approach would also be possible with MC simulations whereby if an electron comes to a halt within the material at some point, then the local potential around that point is adjusted negatively. Similarly if a SE is excited, the positive charge left behind can modify the local potential in the opposite manner. Cornet *et al.* (2008) used a model with a single spatial dimension whereas Li and Zhang (2010a) and Li and Zhang (2010b) (who use a 3D MC model) make assumptions about whether a charge is trapped or not depending on the density of trapped charge. Several methods to tackle this difficult problem have been explored by Amlaki *et al.* (2011). One is the use of the Born approximation where the potential is created from the bound charges which are considered to arise from the perturbation of the system due to the primary electron beam and consider a "particle-mesh" and analytic approaches (Amlaki *et al.*, 2011).

Spin Polarised Measurements

Low energy electrons are more sensitive to the spin state of the material and so are ideally suited to the study of magnetic and spintronic materials. In order to study such materials using low energy electrons one could use a spin polarised electron source or one could determine the spin polarisation of the electrons emerging from the material. Ideally both would be in the same instrument.

Spin Polarised Electron Sources

The preferred choice as a source of spin polarised electrons in many experiments is the GaAs photocathode (Pierce *et al.*, '80). Circularly polarised light is used to preferentially excite one spin orientation. The spin direction can be reversed by changing the sense of the circularly polarised light striking the photocathode. The degree of polarisation can be enhanced by lifting valence band degeneracy through symmetry breaking such as using GaAs/GaP strained layer superlattices (Maruyama *et al.*, 2004). Kuwahara *et al.* (2006) have created a spin

polarised field emission source using a GaAs tip. The same group have used a thin film of GaAs and illuminated it from the back (Jin *et al.*, 2008). This creates a much brighter source than the original GaAs photocathode and has been used as a source of electrons in a Transmission Electron Microscope (TEM) (Kuwahara *et al.*, 2012). Despite these successes, there are problems in operating the GaAs photocathode. The surface needs to have Negative Electron Affinity (NEA) which is implemented by coating with Caesium. This coating needs to be regularly replenished (every $\sim$24 h) and the GaAs photocathode needs to be kept in Extreme High Vacuum (XHV) ($<10^{-11}$ mbar) conditions so as to keep the caesiated surface of the GaAs photocathode in a good condition. \Hence operating such cathodes requires personnel with high expertise and it is also expensive.

An alternative approach to providing a spin polarised field emission is to use field emission tips made from magnetic materials. Spin polarization (with greater than 90% polarization) from EuS coated W tips has been reported (Baum *et al.*, '77). However, the tips had to be cooled to 10 K and maintained in a high magnetic field. Temperatures only marginally above 10 K resulted in the loss of the spin polarization and so these FE sources are not suited for use in SEMs

More recently, room temperature spin polarized FE has been achieved using thin films of magnetic material coated on a W tip (Bryl and Altman, 2003). For instance, Niu and Altman (2010) coated thin Fe and Co films on to W (001) and (111) tips and obtain modest spin polarisations which were also stable. The authors state that the tips could also be used for Scanning Probe Microscopy (SPM) applications. Ultrathin magnetic films coated on W tips have already been used for Spin Polarised Scanning Tunnelling Microscopy (SP-STM) (Wulfhekel and Kirschner, '99; Bode, 2003). One problem with these tips is that it has not proven possible to magnetize the tips in a well-defined direction. Upon flipping the magnetization direction, the magnetization at the tip tends to orient itself along one of the crystallographic easy axes and not in the desired magnetization direction.

The use of spin polarised tips could also be applied in NFESEM and combined with spin polarised detection of BSEs and SEs would make a powerful combination for the study of magnetic materials. Work in this area has already been carried out by Schlenhof (2013) who used antiferromagnetic bulk Cr tips in Near Field Emission mode to study the properties of nano-magnets. However, such antiferromagnetic tips cannot change their direction of magnetization.

Spin Polarised Electron Detectors

The determination of the spin of an electron has many applications in the area of magnetism and spintronics.

The technique of Scanning Electron Microscopy with Polarization Analysis (SEMPA) has been often used in such studies. The measurement of the spin of an electron traveling in free space has traditionally been undertaken by the use of a Mott Polarimeter (Gay and Dunning, '92). This device takes advantage of the spin asymmetry in scattering from high atomic number elements at high electron energy. The spin asymmetry is due to a spin orbit term in the scattering cross-section which causes a spin dependence in the scattering. Usually the electrons to be analysed are accelerated to a high voltage (20–100 keV) and then strike a thin gold film. Detectors are placed either side of the film and detect electrons which are transmitted through the film and scattered towards the detectors. If the detectors are placed to the left and right of the beam striking the gold film and the current detected by each detector is I_L and I_R respectively, then the asymmetry, $A(\theta)$, is given by

$$A(\theta) = \frac{I_R - I_L}{I_R + I_L} \qquad (5)$$

Another important parameter for Spin Polarimeters is the figure of merit (or efficiency), ε, which is given by:

$$\varepsilon = \frac{1}{1_0} S_{eff}^2 \qquad (6)$$

where I is the total scattered current, I_0 is the current entering the polarimeter and S_{eff} is the Sherman function which is a measure of the ability of the polarimeter to measure spin polarization, or,

$$A = S_{eff} P \qquad (7)$$

where P is the spin polarization of the incident beam. Unfortunately the rate at which spin polarised data can be acquired is extremely slow when using a Mott Polarimeter due to its low efficiency which is typically between 10^{-5} and 10^{-4} (Huang et al., '93, 2002).

There have been a number of attempts to improve the sensitivity of spin detection over that of the Mott polarimeter.

Li et al. (2014) have built a solid state device based on spin filtering across a buried 4 nm thick Fe layer. The electrons then cause Cathodoluminescence (CLM) in GaAlAs/GaInAs quantum well structures and the CLM is then detected using a photomultiplier. The Sherman function (efficiency) of the device is estimated to be 10^{-2}, but the device had low light collection efficiency. However, Li et al. (2014) propose improvements to their device which will considerably improve its performance.

Kolbe et al. (2011) make use of the spin asymmetric LEED reflection from the W (100) crystal surface to create a highly parallel detector. They report a four orders of magnitude improvement in sensitivity above the Mott polarimeter. Most of this gain is due to the parallel data acquisition.

Another approach is reported by Okuda et al. (2008). They grow a thin Fe film on a MgO crystal and used Very Low Energy Electron Diffraction (VLEED) to measure the spin of the impacting electron. They achieve a two orders of magnitude improvement over the Mott polarimeter.

It has been suggested to make use of the scattering from empty d states to make a spin polarimeter based on the transmission of electrons through thin films of Fe or Co (Schonhense and Siegmann, '93). However, there are considerable technical difficulties in creating large free standing films of Fe or Co that are only a few nm thick.

One advantage in using a Mott Polarimeter in association with SLEEM is that in SLEEM the electrons which strike the sample surface are reaccelerated to a high voltage prior to being detected. Hence unlike other surface science experiments the returning or transmitted electrons might need only relatively small further acceleration and which could then be passed into a Mott Polarimeter.

Transmission and Reflection Experiments on 2D Materials Using SLEEM

2D materials such as graphene are of current great interest and promise many useful applications. Slow electrons can be used to study the nature of graphene and help to characterise the material in many new ways. For example it has been shown using LEEM that the reflectivity of slow electrons passes through a number of maxima and minima with electron energy (see Fig. 10) (Feenstra et al., 2013). The number of peaks that are

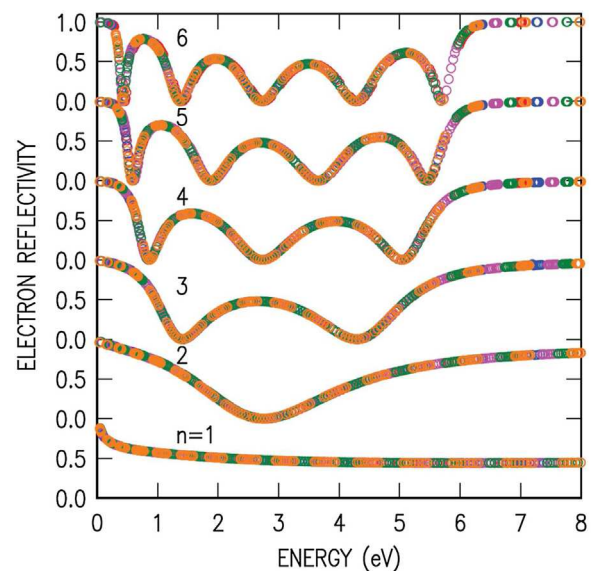Fig 10.   Computed reflectivity for free-standing slabs of n-layer graphene (with permission from (Feenstra et al., 2013)).

observed is equal to the number of graphene layers minus one. These results have been confirmed using SLEEM. The results are in close agreement with theoretical predictions which are made with the help of Density Functional Theory (DFT) (Feenstra and Widom, 2013; Srivastava *et al*., 2013; Gao *et al*., 2015). The successful use of this alternative approach to studying electron transport at low energies suggests there is a limit to the use of MC in electron simulation. It is highly unlikely that the oscillations in electron intensity observed from graphene could be simulated using classical MC approaches.

In addition to the intensity oscillations of the reflected electrons with electron energy, Frank *et al*. (2015) report on measurements of transmission of low energy electrons through thin free standing graphene. No oscillations in intensity for the transmitted beam are found and the transmissivity of the film continues to decrease down to the lowest impact energies. In addition, it was also found that the electron transmissivity reduced over time when high impact energies ($>50\,\mathrm{eV}$) were used. This is consistent with the deposition of carbon contamination often found in SEMs. However, when lower electron energies were used, the transmissivity increased with time—suggesting a low energy electron cleaning effect.

Introducing Quantum Mechanics to Monte Carlo Simulations

Low energy electrons present particular challenges to MC simulations as the wave nature of the electron becomes ever more influential the lower the electron energy that is used. Hence attempts to bring in quantum effects into MC simulations have been made in recently by using the Bohmian Quantum Trajectory method (Zeng and Ding, 2011; Ruan *et al*., 2014) where the electron is modelled according to the quantum theory of Bohm ('52). The authors have simulated the atomic resolution images acquired from SEs (Brown *et al*., 2013) as well as diffraction effects in thin films. Brown *et al*. (2013) have also simulated the atomic resolution images acquired by Zhu *et al*. (2009). The approach taken by Zeng and Ding (2011) and Ruan *et al*. (2014) is considerably more complex than the traditional classical MC approach and would require the band structure and electron wave-functions of the material under study. The Bohmian Quantum Trajectory method is more usually used for Quantum Molecular Dynamics or Quantum Hydrodynamic calculations (Towler, 2011). The Quantum MC (QMC) program CASINO which is used, for example, to carry out Quantum chemistry calculations (Towler, 2011) (not to be confused with the electron transport simulation program of the same name (Demers *et al*., 2011) uses the Quantum Trajectory method. Pseudo potential methods of DFT cannot be used to simulate high energy electrons as these will penetrate into the inner core of atoms due to the use of pseudo-potentials and this is where the DFT programs make their approximations. The more computationally expensive Full Potential methods would need to be used instead. Pseudopotentials have also been employed in QMC to speed up calculations (Towler, 2011), but care in their use for electron transport simulations needs to be taken. Ruan *et al*., 2014) based their method on the well-known TEM multi-slice method and so high angle elastic scattering effects can be ignored.

Future Directions

Improved agreement between Monte Carlo simulations and experimental results for secondary electrons should be sought, starting at higher energies and aiming eventually at energies down to a few eV. Simulation using Monte Carlo will need new approaches in order to accurately replicate the measured results.

Although Monte Carlo has been the basis of electron transport simulation for the interaction of primary beams with samples in SEMs for many years, it would seem at the very lowest energies (below $50\,\mathrm{eV}$), the technique is no longer appropriate and it may well be better to use techniques which take into account the band-structure of the material and the wave nature of the electron as has been espoused by Krasovskii and Strocov (2009), Flege and Krasovskii (2014), and Feenstra and Widom (2013).

Further work needs to be done to determine the nature of the elastic and inelastic mean free paths at low energies. This includes determining the role of scattering from empty d-states in transition metals and clarifying relations among the elastic, inelastic and transport Mean Free Path.

The introduction of new methods aimed at reducing the effect of sample charging are likely to be introduced leading to improved imaging performance in SEMs.

New spin polarised sources which are easier to operate and less costly would be required if spin polarised studies are to be introduced to low energy SEMs on a wide scale.

Due to the surface sensitivity of using a primary beam with low energy electrons, techniques such as SLEEM and NFESEM should be carried out in Ultra High Vacuum for quantitative results.

Overall one can say that progress towards a more quantitative description of low energy electrons in scanning electron microscopes is being made although there are still many hurdles to overcome.

Annex

Given a probability distribution, p(x), of an event happening near to the value of x, we may have a Gaussian bell curve such as that shown in Figure 11.
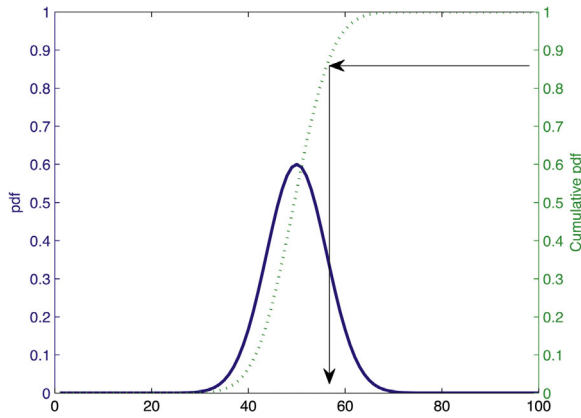
Fig 11. Distribution of probabilities, p(x) around x (blue solid line) and the corresponding cumulative distribution function (green dotted line). The arrows indicate how a random number between 0 and 1 isconverted into the desired probability distribution function.

The integral under the curve p(x) is 1, i.e.

$$\int_0^\infty p(x)dx = 1 \qquad (A1)$$

We now need to determine the cumulative probability distribution function, P(x), which is the likelihood that an event has occurred prior to x.

$$P(x) = \int_0^x p(x')dx' \qquad (A2)$$

Since p(x) is always greater than 0, there is always a one to one mapping from P(x) to x (see Fig. 11). Note that P(x) always lies in the range 0–1. Hence by selecting a random number, R, in the range 0–1 and then finding the value of x such that P(x) = R and then repeating the process many times, the probability distribution that results should replicate p(x). Quite often the function p(x) is not known analytically, so one has a series of
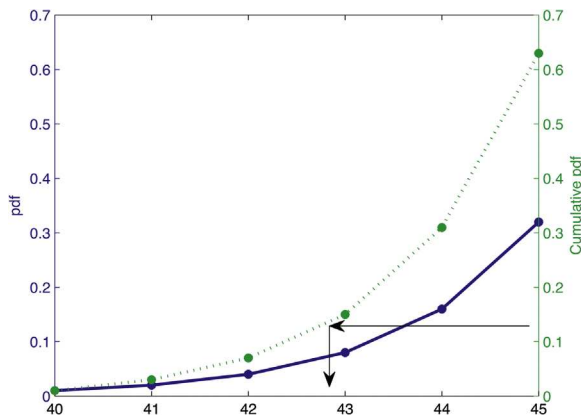

Fig 12. Choosing a random number by linear interpolation between points on a cumulative distributionfunction.

tabulated values. In order to determine values of x which are not tabulated, one could simply interpolate between the tabulated values above and below R. However, if the interpolation is linear between two neighbouring tabulated points (see Fig. 12), then this means that the probability function will not change between the two tabulated values and the resulting function will have a stepped appearance. A better approach might be to use a more accurate form of interpolation such as quadratic or cubic. Sometimes it can be better to choose a method of interpolation which reflects the known behavior of p(x). Hence if a function had the form $y = Bx^n$ where B and n are constants, then it would be better to form the log of y and x as this would create the linear function: $\log(y) = \log(B) + n \log(x)$ and then one could linearly interpolate on this modified function.

Acknowledgments

References

Akkerman A, Barak J, Emfietzoglou D. 2005. Ion and electron track-structure and its effects in silicon: Model and calculations. Nucl Instrum Meth Phys Res B 227:319.

Alkauskas A, Schneider S, Sagmeister S, Ambrosch-Draxl C, Hébert C. 2010. Theoretical analysis of the momentum-dependent loss function of bulk Ag. Ultramicroscopy 110:1081–1086.

Amlaki T, Budko N, Bosch E, et al. 2011. Field of inserted charges during Scanning Electron Microscopy of non-conducting samples. Proc Phys Industry 17–31.

Ashley JC. 1988. Interaction of low-energy electrons with condensed matter: Stopping powers and inelastic mean free paths from optical data. J Elec Spectrosc Rel Phen 46:199–214.

Baroody EM. 1950. A theory of secondary electron emission from metals. Phys Rev 78:780–787.

Barrett N, Krasovskii EE, Themlin J-M, Strocov VN. 2005. Elastic scattering effects in the electron mean free path in a graphite overlayer studied by photoelectron spectroscopy and LEED. Phys Rev B 71:035427.

Batson PE, Silcox J. 1983. Experimental energy-loss function, Im {-1/e(q,w)}, for aluminum. Phys Rev B 27:5224–5239.

Bauer E. 1994. Low energy electron microscopy. Rep Prog Phys 57:895–938.

Baum G, Kisker E, Mahan AH, Raith W, Reihl B. 1977. Field emission of monoenergetic spin-Polarized electrons. Appl Phys 14:149–153.

Bernal MA, Bordage MC, Brown JMC, et al. 2015. Track structure modeling in liquid water: A review of the

Geant4-DNA very low energy extension of the Geant4 Monte Carlo simulation toolkit. Phys Medica 31:861–874.

Binnig G, Rohrer H. 2000. Scanning tunneling microscopy. IBM J Res Dev 44:279–293.

Bode M. 2003. Spin-polarized scanning tunnelling microscopy. Rept Prog Phys 66:523–582.

Bohm D. 1952. A suggested interpretation of the quantum theory in terms of "Hidden" variables. I Phys Rev 85:166–179.

Bourke JD, Chantler CT. 2010. Measurements of electron inelastic mean free paths in materials. Phys Rev Lett 104:206601.

Brown HG, D'Alfonso AJ, Allen LJ. 2013. Secondary electron imaging at atomic resolution using a focused coherent electron probe. Phys Rev B 87:054102.

Bryl R, Altman MS. 2003. Spin-polarized vacuum tunneling in field emission from Co-coated W(111) tips. J Appl Phys 94:4670–4675.

Cazaux J. 2004. Charging in scanning electron microscopy "from inside and outside". Scanning 26:181–203.

Cazaux J. 2005. Recent developments and new strategies in scanning electron microscopy. J Microsc 217:16–35.

Cazaux J. 2010. Calculated influence of work function on SE escape probability and Secondary Electron Emission yield. Appl Surf Sci 257:1002–1009.

Clark SJ, Segall MD, Pickard CJ, et al. 2005. First principles methods using CASTEP. Zeitschrift für Kristallographie 220:567–570.

Cornet N, Gœuriot D, Guerret-Piecourt C, et al. 2008. Electron beam charging of insulators with surface layer and leakage currents. J Appl Phys 103:064110.

Dapor M. 2003. Electron-beam interactions with solids— application of the monte carlo method to electron scattering problems. Springer Verlag Berlin Heidelberg: Springer Tracts in Modern Physics.

Demers H, Poirier-Demers N, Couture AR, et al. 2011. Three-dimensional electron microscopy simulation with the CA-SINO Monte Carlo software. Scanning 33:135–146.

Ding Z-J, Shimizu R. 1996. A monte carlo modelling of electron interaction with solids including cascade secondary electron production. Scanning 18:92–113.

Ding ZJ, Li HM, Goto K, Jiang YZ, Shimizu R. 2004. Energy spectra of backscattered electrons in Auger electron spectroscopy: Comparison of Monte Carlo simulations with experiment. J Appl Phys 96:4598–4606.

Dunaevsky A, Raitses Y, Fisch NJ. 2003. Secondary electron emission from dielectric materials of a Hall thruster with segmented electrodes. Phys Plasmas 10:2574–2577.

Eckhardt R. 1987. Stan Ulam, John von Neumann, and the Monte Carlo method. Los Alamos Sci, Special Issue 15:131–137.

Egerton RF. 1996. Electron energy-loss spectroscopy in the electron microscope. New York: Plenum Press.

El Gomati MM, Walker CGH, Assad AMD, Zadrazil M. 2008. Theory experiment comparison of the electron backscattering factor from solids at low electron energy (250–5,000 eV). Scanning 30:2–15.

El-Gomati MM, Walker CGH. 2014. Towards quantitative scanning electron microscopy. Adv Imaging Electron Phys 183:1–40.

El-Gomati MM, Walker CGH, Zha X. 2011. Towards quantitative scanning electron microscopy: Applications to nano-scale analysis. Nucl Inst Meth Phys Res A 645:68–73.

Elk. 2016. The Elk FP-LAPW Code http://elk.sourceforge.net/

Emfietzoglou D, Cucinotta FA, Nikjoo H. 2005. A complete dielectric response model for liquid water: A solution of the bethe ridge problem. Radiat Res 164:202–211.

Emfietzoglou D, Kyriakou I, Abril I, Garcia-Molina R, Nikjoo H. 2012. Inelastic scattering of low energy electrons in liquid water computed from optical data models of the Bethe surface. Int J Rad Biol 88:22–28.

Emfietzoglou D, Kyriakou I, Abril I, Garcia-Molina R. 2013. The effect of static many-body local-field corrections to inelastic electron scattering in condensed media. J Appl Phys 114:144907.

Feenstra RM, Widom M. 2013. Lo w-energy electron reflectivity from graphene: First-principles computations and approximate models. Ultramicroscopy 130:101–108.

Feenstra RM, Widom M. 2015. WaveTrans: Real-space wave-functions from VASP WAVECAR file. Carnegie Mellon University: http://www.andrew.cmu.edu/user/feenstra/wavetrans/

Feenstra RM, Srivastava N, Gao Q, et al. 2013. Low-energy electron reflectivity from graphene. Phys Rev B 87:041406.

Fermi E. 1940. The ionization loss of energy in gases and in condensed materials. Phys Rev 57:485–493.

Fitting HJ, Touzin M. 2010. Time-dependent start-up and decay of secondary electron emission in dielectrics. J Appl Phys 108:033711.

Flege JI, Krasovskii EE. 2014. Intensity-voltage low-energy electron microscopy for functional materials characterization. Phys Status Solidi RRL 8:463–477.

Frank L, Zadražil M, Müllerová I. 2001. Scanning electron microscopy of nonconductive specimens at critical energies in a cathode lens system. Scanning 23:36–50.

Frank L, Müllerová I, Matsuda K, Ikeno S. 2007. Cathode lens mode of the SEM in materials science applications. Mat Trans 48:944–948.

Frank L, Mikmeková E, Müllerová I, Lejeune M. 2015. Counting graphene layers with very slow electrons. App Phys Lett 106:013117.

Ganachaud JP, Mokrani A. 1995. Theoretical study of the secondary electron emission of insulating targets. Surf Sci 334:329–341.

Gao Q, Mende PC, Widom M, Feenstra RM. 2015. Inelastic effects in low-energy electron reflectvity of two-dimensional materials. J Vac Sci Technol B 33:02B105.

Gay TJ, Dunning FB. 1992. Mott electron polarimetry. Rev Sci Instrum 63:1635–1650.

Goto K, Sakakibara N, Takeichi Y, Numata Y. 1994. True auger spectra shapes: A step to standard spectra. Surf Interf Anal 22:75–78.

Greenwood JC, Prutton M, Roberts RH. 1994. Atomic-number dependence of the secondary electron cascade from solids. Phys Rev B 49:12485–12495.

Grella L, Lorusso G, Niemi T, Adler DL. 2004. Simulations of SEM imaging and charging. Nucl Instrum Meth Phys Res A 519:242–250.

Gulans A, Kontur S, Meisenbichler C, et al. 2014. Exciting—a full-potential all-electron package implementing density-functional theory and many-body perturbation theory. J Phys Condens Matt 26:363202.

Hafner J. 2008. Ab-initio simulations of materials using VASP: Density-functional theory and beyond. Comput Solid State Chem 29:2044–2078.

Hayashi H, Udagawa Y. 2011. Charged particle and photon interactions with matter, recent advances, applications and interfaces. In: Hatano Y, Katsumura Y, Mozumder A, editors. Boca Raton: CRC Press.

Hess K. 1991. Monte Carlo device simulation: Full band and beyond. New York: Springer Science + Business Media.

Huang D-J, Lee J-Y, Suen J-S, et al. 1993. Adapting a compact Mott spin polarimeter to a large commercial electron energy analyzer for spin-polarized electron spectroscopy. Rev Sci Instrum 64:3474–3479.

Huang DJ, Wu WP, Chen J, et al. 2002. Performance of a Mott detector for undulator-based spin-resolved spectroscopy. Rev Sci Instrum 73:3778–3783.

Jablonski A, Powell CJ. 1999. Relationships between electron inelastic mean free paths, effective attenuation lengths, and mean escape depths. J Elect Spec Rel Phen 100:137–160.

Jablonski A, Salvat F, Powell CJ. 2010. NIST electron elastic-scattering cross-section database—Version 3. 2. Gaithersburg, MD: National Institute of Standards and Technology.

Ji Y, Guo HS, Zhong TX, et al. 2005. Charge and charging compensation on oxides and hydroxides in oxygen environmental SEM. Ultramicroscopy 103:191–198.

Jin X, Yamamoto N, Nakagawa Y, et al. 2008. Super-High brightness and high-spin-polarization photocathode. Appl Physi Expr 1:045002.

Joy DC, Luo S. 1989. An empirical stopping power relationship for low-energy electrons. Scanning 11:176–180.

Joy DC. 1991. An introduction to monte carlo simulations. Scanning Microsc 5:329–337.

Joy DC. 1995. Monte Carlo modeling for electron microscopy and microanalysis. Oxford, New York: Oxford University Press.

Khalid R, Salvat Pujol F, Werner WSM. 2013. Secondary electron energy loss coincidence (e,2e) spectroscopy on Ag and Si surfaces. J Phys Conf Ser 439:012003.

Khursheed A. 2010. Scanning Electron Microscope Optics and Spectrometers: World Scientific.

Kieft E, Bosch E. 2008. Refinement of Monte Carlo simulations of electron-specimen interaction in low-voltage SEM. J Phys D Appl Phys 41:215310.

Kirk TL 2010. Near Field Emission Scanning Electron Microscopy: ETH Zurich.

Kite J, Davies RE, Dennison JR. 2002. Angular dependence of secondary electron emission spectra from a polycrystalline Au surface. Bull Am Phys Soc 47:370.

Kolbe M, Lushchyk P, Petereit B, et al. 2011. Highly efficient multichannel spin-Polarization detection. Phys Rev Lett 107:207601.

Krasovskii EE, Strocov VN. 2009. Very-low-energy electron diffraction from TiS 2: Experiment and ab initio theory. J Phys Condens Matt 21:314009.

Kuwahara M, Nakanishi T, Okumi S, et al. 2006. Field emission of spin-polarized electrons extracted from photoexcited GaAs tip. Jap J App Phys 45:6245–6249.

Kuwahara M, Kusunoki S, Jin XG, et al. 2012. 30-kV spin-polarized transmission electron microscope with GaAs-GaAsP strained superlattice photocathode. App Phys Lett 101:033102.

Li HM, Ding ZJ. 2005. A Monte Carlo simulation of secondary electron and backscattered electron images in scanning electron microscopy. Acta Met A Sin 18:351–355.

Li W-Q, Zhang H-B. 2010a. The positive charging effect of dielectric films irradiated by a focused electron beam. Appl Surf Sci 256:3482–3492.

Li W-Q, Zhang H-B. 2010b. The surface potential of insulating thin films negatively charged by a low-energy focused electron beam. Micron 41:416–422.

Li YG, Mao SF, Ding ZJ. 2011. Monte Carlo simulation of SEM and SAM images, chapter 11 in "Applications of Monte Carlo method in science and engineering". In: Mordechai S, editor. Rijeka, Croatia - EUROPEAN UNION: Intech.

Li X, Tereshchenko OE, Majee S, et al. 2014. Optical detection of spin-filter effect for electron spin polarimetry. App Phys Lett 105:052402.

Lin Y, Joy DC. 2005. A new examination of secondary electron yield data. Surf Interf Anal 37:895–900.

Müllerová I, Frank L. 2003. Scanning low-Energy electron microscopy. Adv Imag Electr Phys 128:309–443.

Müllerová I, Frank L. 2007. Very low energy scanning electron microscopy. Modern research and educational topics on microscopy. Microscopy series No. 3, vol. 2. Badajoz, Spain: Formatex. p 795–804.

Müllerová I, Hovorka M, Konvalina I, Uncovsky M, Frank L. 2011. Scanning transmission low-energy electron microscopy. IBM J Res Dev 55:2.

Müllerová I. 1999. Imaging of specimens at optimized low and very low energies in scanning electron microscopy. Scanning Microsc 13:7–22.

Maruyama T, Luh D-A, Brachmann A, et al. 2004. Systematic study of polarized electron emission from strained GaAs/ GaAsP superlattice photocathodes. App Phys Lett 85:2640–2642.

Matthew JAD, Prutton M, El Gomati MM, Peacock DC. 1988. The spectral background in electron excited auger electron spectroscopy. Surf Interf Anal 11:173–181.

McKay KG. 1948. Secondary electron emission. Adv Electr. I:66.

Mermin N. 1970. Lindhard dielectric function in the relaxation-time approximation. Phys Rev B 1:2362–2363.

Metropolis N. 1987. The beginning of the monte carlo method. Los Alamos Sci Special Issue 15:125–130.

Mikaelian T., 2001. Spacecraft Charging and Hazards to Electronics in Space. Ontario, Canada: York University Press.

Mott NF, Massey HSW. 1949. The theory of atomic collisions. Oxford: Clarendon Press.

Niu YR, Altman MS. 2010. Spin polarized field emission from Fe and Co-coated W tips. Surf Sci 604:1055–1059.

Okuda T, Takeichi Y, Maeda Y, et al. 2008. A new spin-polarized photoemission spectrometer with very high efficiency and energy resolution. Rev Sci Instrum 79:123117.

Overton N, Coleman PG. 1997. Measurement of the energy spectrum of secondary electrons ejected from solids by positron impact. Phys Rev Lett 79:305–308.

Palik E. 1998. Handbook of optical constants of solids,3. London: Academic Press.

Pendry J, 1974. Low energy electron diffraction: The theory and its application to determination of surface structure. London, New York: Academic Press.

Penn DR. 1987. Electron mean-free-path calculations using a model dielectric function. Phys Rev B 35:482–486.

Pescia D. 2015. Personal communication. Switzerland: EtH Zurich.

Pierce DT, Celotta RJ, Wang G-C. 1980. GaAs spin polarized electron source. Rev Sci Instrum 51:478–499.

Pivi MTF, Furman MA. 2003. Electron cloud development in the proton storage ring and in the spallation neutron source. Phys Rev ST Accel Beams 6:034201.

Pokorná Z, Mikmeková Š, Müllerová I, Frank L. 2012. Characterization of the local crystallinity via reflectance of very slow electrons. Appl Phys Lett 100:261602.

Powell CJ. 1967. Inelastic scattering of kilovolt electrons by solids and liquids: Determination of energy losses, cross sections, and correlations with optical data. Health Phys 13:1265–1275.

Reimer L. 1985. Scanning electron microscopy. In: Hawkes P, editor. Berlin: Springer.

Ritchie RH, Howie A. 1977. Electron excitation and the optical potential in electron microscopy. Phil Mag 36:463–481.

Ritchie RH. 1959. Interaction of charged particles with a degenerate Fermi-Dirac electron gas. Phys Rev 114:644–654.

Ruan Z, Zhang M, Zeng RG, et al. 2014. Simulation study of the atomic resolution secondary electron imaging. Surf Interf Anal 46:1296–1300.

Salvat F, Fernandez-Varea JM, Acosta E, Sempau J, 2001. PENELOPE, A Code System for Monte Carlo Simulation of Electron and Photon Transport", Proceedings of a Workshop/ Training Course, OECD/NEA 5–7 November 2001: NEA/ NSC/DOC.

Schlenhof A. 2013. Imaging and switching individual nano-magnets with spin-polarized scanning field emission microscopy. Hamburg: Universität Hamburg.

Schonhense G, Siegmann HC. 1993. Transmission of electrons through ferromagnetic material and applications to detection of electron spin polarization. Ann Physik 2:465–474.

Schreiber E, Fitting H-J. 2002. Monte Carlo simulation of secondary electron emission from the insulator SiO2. J Elec Spec Rel Phen 124:25–37.

Seah MP, Dench WA. 1979. Quantitative electron spectroscopy of surfaces: A standard data base for electron inelastic mean free paths in solids. Surf Interf Anal 1:2–11.

Sickafus EN. 1977. Linearized secondary-electron cascades from the surfaces of metals. I. Clean surfaces of homogeneous specimens. Phys Rev B 16:1436–1447.

Siegmann HC. 1992. Surface and 2D magnetism. J Phys Condens Matt 4:8395–8434.

Srivastava N, Gao Q, Widom M, et al. 2013. Low-Energy electron reflectivity of graphene on copper and other substrates. Phys Rev B 87:245414.

Starý V, Zemek J, Pavluch J. 2008. Angular and energy distribution of backscattered electrons simulated by Monte Carlo—assessment by experiment I. Vacuum 21:121–124.

Tanuma S, Powell CJ, Penn DR. 2005. Calculations of electron inelastic mean free paths VIII. Data for 15 elemental solids over the 50-2000eV range. Surf Interf Anal 37:1–14.

Thong JTL, Lee KW, Wong WK. 2001. Reduction of charging effects using vector scanning in the scanning electron microscope. Scanning 23:395–402.

Tilinin IS, Werner WSM. 1993. Angular and energy distribution of Auger and photoelectrons escaping from non-crystalline solid surfaces. Surf Sci 290:119–133.

Towler M. 2011. Quantum Monte Carlo, or, how to solve the many-particle Schrödinger equation accurately whilst retaining favourable scaling with system size. Computational Methods for Large Systems: Electronic Structure Approaches for Biotechnology and Nanotechnology: Wiley.

Valentin A, Raine M, Sauvestre J-E, Gaillardin M, Paillet P. 2012. Geant4 physics processes for microdosimetry simulation: Very low energy electromagnetic models for electrons in Silicon. Nucl Instrum Meth Phys Res B 288:66–73.

Villarrubia JS, Ritchie NWM, Lowney JR. 2007. Monte Carlo modeling of secondary electron imaging in three dimensions. Proc of SPIE 6518. 65180K-1–65180K-14.

Vos M. 2016. A model dielectric function for low and very high momentum transfer. Nucl Instrum Meth Phys Res B 366:6–12.

Walker CGH, El-Gomati MM, Assa'd AMD, Zadražil M. 2008. The secondary electron emission yield for 24 solid elements excited by primary electrons in the range 250-5000eV: A Theory/Experiment comparison. Scanning 30:365–380.

Walker CGH, El-Gomati MM, Matthew JAD. 2009. Recent developments in the understanding and application of backscattered and secondary electrons in the SEM. Proc SPIE 7378:73780Z.

Walker CGH, Matthew JAD, El-Gomati MM. 2014. The sensitivity of backscattering coefficients to elastic scattering cross-sections and electron stopping powers. Scanning 36:241–245.

Walker CGH, Konvalina I, Mika F, Frank L. 2016. Quantitative comparison of simulated and measured signals in the STEM mode of a SEM. Ultramicroscopy Submitted.

Weissker H-C, Serrano J, Huotari S, et al. 2010. Dynamic structure factor and dielectric function of silicon for finite momentum transfer: Inelastic x-ray scattering experiments and ab initio calculations. Phys Rev 81:085104.

Werner W, Glantschnig K, Ambrosch-Draxl C. 2009. Optical constants and inelastic electron-scattering data for 17 elemental metals. J Phys Chem Ref Data 38:1013–1092.

Werner WSM, Salvat-Pujol F, Bellissimo A, et al. 2013. Secondary-electron emission induced by in vacuo surface excitations near a polycrystalline Al surface. Phys Rev B 88:201407.

Werner WSM. 2001. Electron transport in solids for quantitative surface analysis. Surf Interface Anal 31:141–176.

Wilkinson AJ, Britton TB. 2012. Strains, planes, and EBSD in materials science. Mater Today 15:366–376.

Winkelmann A, Trager-Cowan C, Sweeney F, Day AP, Parbrook P. 2007. Many-beam dynamical simulation of electron backscatter diffraction patterns. Ultramicroscopy 107:414–421.

Wulfhekel W, Kirschner J. 1999. Spin-polarized scanning tunneling microscopy on ferromagnets. Appl Phys Lett 75:1944–1946.

Young R, Ward J, Scire F. 1972. The topografiner: An instrument for measuring surface microtopography. Rev Sci Instrum 43:999–1011.

Yubero F, Sanz J, Ramskov B, Tougaard S. 1996. Model for quantitative analysis of reflection-electron-energy-loss spectra: Angular dependence. Phys Rev B 53:9719–9727.

Zanin DA, Cabrera H, De Pietro LG, et al. 2012. Fundamental aspects of near-Field emission scanning electron microscopy. Adv Imag Electr Phys 170:227–258.

Zdyb R, Bauer E. 2013. Spin-resolved inelastic mean free path of slow electrons in Fe. J Phys Condens Matt 25:272201.

Zeng RG, Ding ZJ. 2011. Simulation study of electron scattering in crystalline solid by using bohmian quantum trajectory method. J Surf Anal 17:198–202.

Zhu Y, Inada H, Nakamura K, Wall J. 2009. Imaging single atoms using secondary electrons with an aberration-corrected electron microscope. Nat Mat 8:808–812.

Zhukov VP, Usuda M, Chulkov EV, Echenique PM. 2003. Dielectric functions and quasi-particle lifetimes in Ag: Full-potential LMTO and LAPW GW approaches. J Elect Spectrosc Rel Phen 129:127–131.

Ziman JM. 1956. The general variational principle of transport theory. Can J Phys 34:1256–1273.